

NUMERICAL ALGORITHM FOR CALCULATING THE GENERALIZED MITTAG-LEFFLER FUNCTION*

HANSJÖRG SEYBOLD[†] AND RUDOLF HILFER[‡]

Abstract. A numerical algorithm for calculating the generalized Mittag-Leffler $E_{\alpha,\beta}(z)$ function for arbitrary complex argument z and real parameters $\alpha > 0$ and $\beta \in \mathbb{R}$ is presented. The algorithm uses the Taylor series, the exponentially improved asymptotic series, and integral representations to obtain optimal stability and accuracy of the algorithm. Special care is applied to the limits of validity of the different schemes to avoid instabilities in the algorithm.

Key words. special functions of mathematical physics, fractional calculus, generalized Mittag-Leffler functions, numerical algorithms

AMS subject classifications. 65D15, 65D20, 33E12, 30E10

DOI. 10.1137/070700280

1. Introduction. The (generalized) Mittag-Leffler function $E_{\alpha,\beta}(z)$ is an entire function with two parameters α and β . The function $E_{\alpha,1}(z)$ is named after Mittag-Leffler, who introduced it in 1903 in a publication on Laplace–Abel integrals [10, 11, 12]. Shortly after its introduction it was generalized by Wiman [21].

The generalized Mittag-Leffler function with a nonnegative argument is completely monotone if and only if $0 < \alpha \leq 1$, $\operatorname{Re}(\beta) \geq \alpha$ [18].

In the special case $\beta = 1$ and $0 < \alpha \leq 1$, complete monotonicity was already conjectured by Feller and later proved by Pollard in 1948 [2, 16]. Analytical investigations on the distribution of the zeros in the complex plane were published by Wiman [21, 22], and numerical results are given in [7, 19].

In recent years fractional calculus has become a popular topic in physics and engineering [8]. Fractional equations of motion are widely accepted for describing viscoelasticity and anomalous diffusion [5, 6, 8, 9, 24]. The generalized Mittag-Leffler function plays a central role in fractional calculus and its applications because it is closely related to the eigenfunction of the fractional derivative operator [8, 17]. Progress in this field requires the calculation of the exact numerical values of the generalized Mittag-Leffler function for arbitrary complex arguments and the study of its properties.

The Mittag-Leffler function shows very different behaviors in the complex plane with varying parameters α and β , so different approaches have to be used for different regions in the complex plane. We present a stable and robust numerical method based on recursion relations, exponentially improved asymptotics, and integral representations for calculating the generalized Mittag-Leffler function for real parameters $\alpha > 0$ and β and arbitrary complex argument z .

The article is organized as follows: First, we give an overview of the formulas used for the calculation in section 2 and introduce the partitioning of the complex plane in section 3. Then, we present the error estimates starting with the series expansions

*Received by the editors August 17, 2007; accept for publication (in revised form) June 12, 2008; published electronically October 24, 2008.

<http://www.siam.org/journals/sinum/47-1/70028.html>

[†]Computational Physics for Engineering Materials, IfB, ETH Zurich, 8093 Zurich, Switzerland (hseybold@ethz.ch).

[‡]ICP, Universität Stuttgart, Pfaffenwaldring 27, 70569 Stuttgart, Germany, and Institut für Physik, Universität Mainz, 55099 Mainz, Germany (hilfer@icp.uni-stuttgart.de).

(section 4). Finally, we discuss the numerical details of the algorithm in section 5 and present the results of extensive numerical calculations in the last section (section 6), comparing the speed and stability of the algorithm.

2. Overview. This section gives an overview of the numerical algorithm. The generalized Mittag-Leffler function is an entire function defined by the following power series:

$$(2.1) \quad E_{\alpha,\beta}(z) = \sum_{k=0}^{\infty} \frac{z^k}{\Gamma(\alpha k + \beta)}$$

for $z \in \mathbb{C}$, $\alpha > 0$, and $\beta \in \mathbb{R}$. If $|z| < 1$, finitely many terms of the power series are sufficient to approximate $E_{\alpha,\beta}(z)$ with arbitrary precision. The error estimates are given in section 4.

The case $\alpha \geq 1$ will be reduced to the case $\alpha < 1$ using the following recursion relation [2, 15]:

$$(2.2) \quad E_{\alpha,\beta}(z) = \frac{1}{2m+1} \sum_{h=-m}^m E_{\alpha/(2m+1),\beta} \left(z^{1/(2m+1)} e^{2\pi i h/(2m+1)} \right),$$

which is valid for all $\alpha, \beta \in \mathbb{R}$, $z \in \mathbb{C}$, and $m = [(\alpha - 1)/2] + 1$. Here $[x]$ denotes the largest integer less than or equal to x .

For large values $|z| \gg 1$ the exponentially improved asymptotic series with the Berry-type smoothing transition gives a fast approximation of the Mittag-Leffler function. If $|\arg(z)| > \pi\alpha$, the asymptotic series is given by [2]

$$(2.3) \quad E_{\alpha,\beta}(z) \sim - \sum_{k=1}^{\infty} \frac{z^{-k}}{\Gamma(\beta - \alpha k)},$$

while for $|\arg(z)| < \pi\alpha$ we find the following series:

$$(2.4) \quad E_{\alpha,\beta}(z) \sim \frac{1}{\alpha} z^{(1-\beta)/\alpha} e^{z^{1/\alpha}} - \sum_{k=1}^{\infty} \frac{z^{-k}}{\Gamma(\beta - \alpha k)}.$$

In the transition area around the Stokes lines $|\arg(z)| < \pi\alpha \pm \delta$, with $\delta < \pi\alpha/2$, we have the Berry-type smoothing given by

$$(2.5) \quad E_{\alpha,\beta}(z) \sim \frac{1}{2\alpha} z^{(1-\beta)/\alpha} e^{z^{1/\alpha}} \operatorname{erfc} \left(-c(\theta) \sqrt{|z|^{1/\alpha}/2} \right) - \sum_{k=1}^{\infty} \frac{z^{-k}}{\Gamma(\beta - \alpha k)}$$

around the lower Stokes line for $-3\pi\alpha/2 < \arg(z) < \pi\alpha/2$, where the parameter c is given by the relation $\frac{1}{2}c^2 = 1 + i\theta - e^{i\theta}$, with $\theta = \arg(z^{1/\alpha}) + \pi$ and the principle branch of c is chosen such that $c \approx \theta + \frac{i}{6}\theta^2 - \frac{1}{36}\theta^3$ for small θ [23]. Around the upper Stokes line $\pi\alpha/2 < \arg(z) < 3\pi\alpha/2$, one finds that

$$(2.6) \quad E_{\alpha,\beta}(z) \sim \frac{1}{2\alpha} z^{(1-\beta)/\alpha} e^{z^{1/\alpha}} \operatorname{erfc} \left(c(\theta) \sqrt{|z|^{1/\alpha}/2} \right) - \sum_{k=1}^{\infty} \frac{z^{-k}}{\Gamma(\beta - \alpha k)},$$

with $\frac{1}{2}c^2 = 1 + i\theta - e^{i\theta}$, $\theta = \arg(z^{1/\alpha}) - \pi$, and the same condition as before for small θ . This exponentially improved asymptotic series converges very rapidly for most values of $z \in \mathbb{C}$, with $|z| > 1$. The Stokes phenomenon and the Berry-type

smoothing for the Mittag-Leffler function have been investigated recently in [13, 23].

In an intermediate range $r_0 \leq |z| \leq r_1$ between the Taylor series and the asymptotic expansion, we use Wiman's integral representation [2, p. 210]

$$(2.7) \quad E_{\alpha,\beta}(z) = \frac{1}{2\pi i} \int_{\mathcal{C}} \frac{y^{\alpha-\beta} e^y}{y^\alpha - z} dy$$

for calculating $E_{\alpha,\beta}(z)$. The values r_0 where the Taylor series ends and r_1 where the asymptotic series starts will be specified later. The path of integration \mathcal{C} in the complex plane starts and ends at $-\infty$ and encircles the circular disc $|y| \leq |z|^{1/\alpha}$ in the positive sense. Equation (2.7) can be obtained by inserting the Hankel representation of the inverse Γ -function into the Taylor series and bending the contour in the complex plane.

3. Partitioning of the complex plane. In different regions of the complex plane the Mittag-Leffler function shows different kinds of behavior. Therefore different calculation schemes are needed for different regions. The following definitions are used to describe these regions. First,

$$(3.1) \quad \overline{\mathbb{D}(r)} = \{z \in \mathbb{C} : |z| \leq r\}$$

is the closure of the open disk $\mathbb{D}(r) = \{z \in \mathbb{C} : |z| < r\}$ of radius r centered at the origin. Next, we define the wedges

$$(3.2) \quad \mathbb{W}(\phi_1, \phi_2) = \{z \in \mathbb{C} : \phi_1 < |\arg(z)| < \phi_2\},$$

$$(3.3) \quad \overline{\mathbb{W}(\phi_1, \phi_2)} = \{z \in \mathbb{C} : \phi_1 \leq |\arg(z)| \leq \phi_2\},$$

where $\phi_2 - \phi_1$ is the opening angle measured in a positive sense and $\phi_1, \phi_2 \in (-\pi, \pi)$. On a disc

$$(3.4) \quad \mathbb{G}_0 = \overline{\mathbb{D}(r_0)}$$

of radius $r_0 < 1$, the Taylor series (2.1) gives a good approximation of the generalized Mittag-Leffler function. For the algorithm we choose $r_0 = 0.95$.

For large values of $|z| \in \mathbb{C}$ exponentially improved asymptotics can be used to calculate $E_{\alpha,\beta}(z)$. Equation (2.4) is used for z in

$$(3.5) \quad \mathbb{G}_1 = [\mathbb{C} \setminus \mathbb{D}(r_1)] \cap \mathbb{W}(-\pi\alpha + \delta, \pi\alpha - \delta)$$

and (2.3) for z in

$$(3.6) \quad \mathbb{G}_2 = [\mathbb{C} \setminus \mathbb{D}(r_1)] \cap \mathbb{W}(\pi\alpha + \tilde{\delta}, -\pi\alpha - \tilde{\delta}),$$

where $r_1 > r_0$ will be defined in (4.21) and δ and $\tilde{\delta}$ are numbers smaller than $\pi\alpha/2$. In the algorithm δ and $\tilde{\delta}$ are chosen to be

$$(3.7) \quad \delta = \pi\alpha/8 \quad \text{and} \quad \tilde{\delta} = \min\{\pi\alpha/8, (\pi + \pi\alpha)/2\}.$$

Close to the Stokes lines $|\arg(z)| = \pi\alpha$, the approximation scheme with the series (2.3) and (2.4) becomes unstable, so the Berry-type smoothed asymptotic series (2.6) is used in the area around the upper Stokes line

$$(3.8) \quad \mathbb{G}_3 = [\mathbb{C} \setminus \mathbb{D}(r_1)] \cap \overline{\mathbb{W}(\pi\alpha - \delta, \pi\alpha + \tilde{\delta})}$$

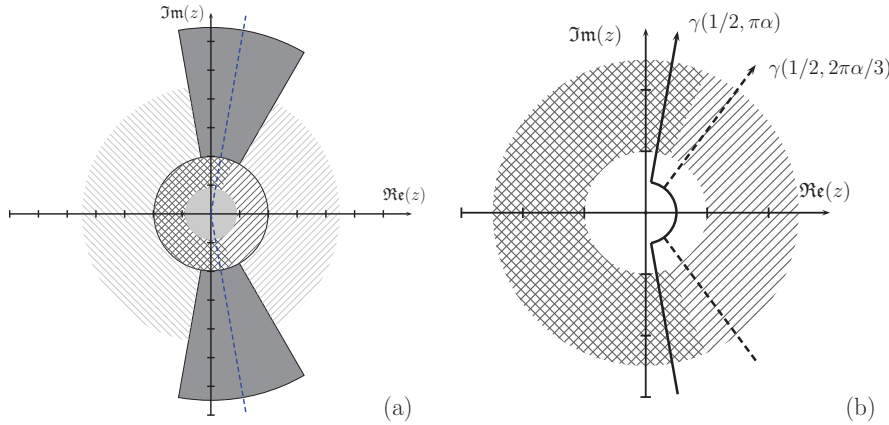


FIG. 1. Figure (a) shows the partitioning of the complex plane for calculating the generalized Mittag-Leffler function $E_{\alpha,\beta}(z)$. The thick dashed lines mark the Stokes line at $\arg(z) = \pm\pi\alpha$. In the central light gray region \mathbb{G}_0 , finitely many terms of the Taylor series (2.1) give a good approximation for the generalized Mittag-Leffler function. The black crosshatched region marks \mathbb{G}_6 (left) and the black hatched one \mathbb{G}_5 (right), where the integral representations (4.31), (4.32) and (4.25), (4.26), respectively, are used for the calculations. The asymptotic series (2.4) and (2.3) are used in the gray hatched regions \mathbb{G}_1 (left) and \mathbb{G}_2 (right). Berry-type smoothing is applied in the gray solid areas: (2.6) in the upper region \mathbb{G}_3 and (2.5) in the lower one \mathbb{G}_4 . In (b) the integration contours for the two cases $\vartheta = \pi\alpha$ (solid line) and $\vartheta = 2\pi\alpha/3$ (dashed line) are shown. While (4.25) and (4.26) are used in the crosshatched region corresponding to (\mathbb{G}_6) , (4.31) and (4.32) are used for the part where the hatching runs at 45° (\mathbb{G}_5).

and (2.5) close to the lower one

$$(3.9) \quad \mathbb{G}_4 = [\mathbb{C} \setminus \mathbb{D}(r_1)] \cap \overline{\mathbb{W}}(-\pi\alpha - \tilde{\delta}, -\pi\alpha + \delta).$$

In the transition area between the Taylor series and the asymptotic expansion, we make use of Hankel's integral representation for the generalized Mittag-Leffler function (2.7). We employ two different contour paths to avoid numerical problems which arise in other algorithms [4] when z is too close to the contour path. The two regions \mathbb{G}_5 and \mathbb{G}_6 are defined by

$$(3.10) \quad \mathbb{G}_5 = \mathbb{D}(r_1) \cap \overline{\mathbb{W}}(-5\pi\alpha/6, 5\pi\alpha/6) \setminus \mathbb{G}_0,$$

$$(3.11) \quad \mathbb{G}_6 = \mathbb{D}(r_1) \cap \mathbb{W}(5\pi\alpha/6, -5\pi\alpha/6) \setminus \mathbb{G}_0,$$

where $\overline{\mathbb{W}}(-5\pi\alpha/6, 5\pi\alpha/6)$ and $\mathbb{W}(5\pi\alpha/6, -5\pi\alpha/6)$ are defined as in (3.3) and (3.2), respectively. The different regions are shown in Figure 1.

4. Error estimates.

4.1. Taylor series. For $z \in \mathbb{G}_0$ finitely many terms of the Taylor series are sufficient to approximate the generalized Mittag-Leffler function for arbitrary $\alpha > 0$ and $\beta \in \mathbb{R}$. The maximum number of terms N taken into account is chosen such that the error

$$(4.1) \quad R_N(z) = \left| E_{\alpha,\beta}(z) - \sum_{k=0}^N \frac{z^k}{\Gamma(\alpha k + \beta)} \right| \leq \varepsilon$$

is smaller than a given accuracy ε .

THEOREM 4.1. *Let $\varepsilon > 0$. If $|z| < 1$ and*

$$(4.2) \quad N \geq \max \left\{ [(2 - \beta)/\alpha] + 1, \left\lceil \frac{\ln(\varepsilon(1 - |z|))}{\ln(|z|)} \right\rceil + 1 \right\},$$

then the error term $R_N(z) = |\sum_{k=N}^{\infty} \frac{z^k}{\Gamma(\alpha k + \beta)}|$ is smaller than the given accuracy ε .

We have $1/\Gamma(x) > 1$ for all $x > 2$. Setting $x = \alpha k + \beta$ one finds that $\frac{1}{\Gamma(\alpha N + \beta)} \leq 1$ for all $N \geq \lceil \frac{2-\beta}{\alpha} \rceil + 1$, where $[a]$ is the smallest integer larger than a ; thus

$$(4.3) \quad R_N(z) = \left| \sum_{k=N}^{\infty} \frac{z^k}{\Gamma(\alpha k + \beta)} \right| \leq \left| \sum_{k=N}^{\infty} z^k \right| \leq \sum_{k=N}^{\infty} |z^k|.$$

Under the condition $|z| < 1$ the geometric series can be summed up, and one obtains together with (4.1) that

$$(4.4) \quad R_N(z) \leq \sum_{k=N}^{\infty} |z^k| = \frac{|z|^N}{1 - |z|} \stackrel{!}{\leq} \varepsilon \quad \text{and therefore} \quad N \geq \frac{\ln(\varepsilon(1 - |z|))}{\ln(|z|)}. \quad \square$$

For the algorithm we have chosen

$$(4.5) \quad M = \max \left\{ \left\lceil \frac{2 - \beta}{\alpha} \right\rceil + 1, \left\lceil \frac{\ln(\varepsilon(1 - |z|))}{\ln(|z|)} \right\rceil + 1 \right\}$$

for the maximum numbers of coefficients that have to be taken into account to reach an accuracy of ε .

4.2. Exponentially improved asymptotics. In this section we give an estimate of the error term of the asymptotic series. To apply the asymptotic series expansions for a given accuracy ε , two parameters have to be determined, which are the truncation point N of the series and a lower limit r_1 of $|z|$ such that the error is smaller than ε for $|z| > r_1$.

THEOREM 4.2. *Let $\alpha \in (0, 1)$. For $N \approx \frac{1}{\alpha}|z|^{1/\alpha}$ and $|z| \geq (-2 \log \frac{\varepsilon}{C})^\alpha$ the estimate of the error term of the asymptotic series (2.3) and (2.4) fulfills the condition*

$$(4.6) \quad R_N(z) = \left| E_{\alpha,\beta}(z) - \left(- \sum_{k=1}^{N-1} \frac{z^{-k}}{\Gamma(\beta - \alpha k)} \right) \right| \leq \varepsilon,$$

where C is a constant dependent only on α, β , and

$$(4.7) \quad R_N(z) = \frac{z^{N-1}}{2\pi i} \int_C \frac{t^{N\alpha-\beta} e^t}{t^\alpha - z} dt.$$

C is the classical Hankel contour, which runs along the positive real axis in the upper half-plane starting from $+\infty + i0$ encircling the origin and returning to $+\infty - i0$ along the positive real axis in the lower half-plane.

Without loss of generality we can assume that $\alpha N - \beta > -1$ by choosing N large enough. Then the circle can be shrunk to zero, and there remain two rays, above and below the cut of the complex plane along the negative real axis. Inserting $t = v e^{-\pi v}$ for the upper part of the contour and $t = v e^{\pi v}$ for the lower one, we obtain

$$(4.8) \quad R_N(z) = L_N(z) + U_N(z),$$

where

$$(4.9) \quad L_N(z) = e^{i\pi\beta} (z e^{i\pi\alpha})^{-N+1} \frac{1}{2\pi i} \int_0^\infty \frac{v^{\alpha N - \beta} e^{-v}}{v^\alpha - z e^{i\pi\alpha}} dv$$

and

$$(4.10) \quad U_N(z) = -e^{-i\pi\beta} (z e^{-i\pi\alpha})^{-N+1} \frac{1}{2\pi i} \int_0^\infty \frac{v^{\alpha N - \beta} e^{-v}}{v^\alpha - z e^{-i\pi\alpha}} dv$$

are the integrals along the upper and lower parts, respectively, of the remaining contour path. Following the arguments in [23] we obtain

$$(4.11) \quad U_N(z) \leq \frac{1}{2\pi \sin \alpha\pi} |z|^{-N} \Gamma(\alpha N - \beta + 1)$$

and similarly

$$(4.12) \quad L_N(z) \leq \frac{1}{2\pi \min\{\sin \alpha\pi, \sin \xi\}} |z|^{-N} \Gamma(\alpha N - \beta + 1),$$

where $\arg(z) \in (-\pi, -\pi\alpha - \xi)$ for $\xi > 0$. The angle ξ describes the distance of z to the Stokes line. Applying the argument of Boyd [1] yields

$$(4.13) \quad L_N(z) \leq C_1(\alpha, \beta) |z|^{-N} \Gamma(\alpha N - \beta + 1) \sqrt{N},$$

where C_1 now depends only on α and β . Combining (4.11) and (4.13) yields

$$(4.14) \quad R_N(z) \leq C_2(\alpha, \beta) |z|^{-N} \Gamma(\alpha N - \beta + 1) \sqrt{N},$$

where we used the fact that $N > 1$ and hence $\sqrt{N} > 1$.

To obtain an estimate for N and a minimal $|z|$, further approximations have to be applied. Using Stirling's formula for $R_N(z)$, (4.14) yields

$$(4.15) \quad \begin{aligned} R_N(z) &\leq C_2(\alpha, \beta) |z|^{-N} \Gamma(\alpha N - \beta + 1) \sqrt{N} \\ &= C_2(\alpha, \beta) |z|^{-N} (\alpha N - \beta) \Gamma(\alpha N - \beta) \sqrt{N} \\ &\leq C_3(\alpha, \beta) |z|^{-N} \sqrt{N} (\alpha N - \beta)^{(\alpha N - \beta + 3/2)} e^{-(\alpha N - \beta)}, \end{aligned}$$

with constant C_3 depending only on α and β . For $\beta \geq 0$ one has $(\alpha N - \beta) \leq \alpha N$. For $\beta < 0$ one obtains $(\alpha N - \beta)^\gamma \leq C'(\alpha N)^\gamma$ by applying the binomial series. Here γ was used as an abbreviation for $(\alpha N - \beta + 3/2)$. Combining these estimates with (4.15) we arrive at

$$(4.16) \quad R_N(z) \leq C_4(\alpha, \beta) (\alpha N)^{1-\beta} e^{N(-\alpha + \alpha \log(\alpha N) - \log |z|)},$$

where we applied the trivial identity $\sqrt{N} = (\alpha N)^{1/2} / \sqrt{\alpha}$ and C_4 absorbs all constants from the approximations. An optimal truncation should be obtained when

$$(4.17) \quad N \approx \frac{1}{\alpha} |z|^{1/\alpha},$$

which yields for real α and β

$$(4.18) \quad R_N(z) \leq C_4(\alpha, \beta)(\alpha N)^{1-\beta} e^{-N\alpha}.$$

Assuming that $|z| > 1$ yields $(|z|^{1/\alpha})^{1-\beta} \leq (|z|^{1/\alpha})^{|1-\beta|}$. Now we apply the inequality $x^y \leq (qy)^y e^{x/q}$, with $x, y, q > 0$ (see Theorem 4.4 below) for $q = 1/2$, $x = |z|^{1/\alpha}$, and $y = |1 - \beta|$. Thus the estimate

$$(4.19) \quad R_N(z) \leq C e^{-\frac{1}{2}|z|^{1/\alpha}}$$

holds for all α, β , and $|z| > 1$, where C is given by $C = C_4(\alpha, \beta)(1/2 \cdot |1 - \beta|)^{|1-\beta|}$. This can now be easily solved for $|z|$ to determine r_1 if we assume that the error $R_N(z)$ is smaller than a given error ε for $|z| > r_1$. Thus we obtain

$$(4.20) \quad |z| \geq r_1 = \left(-2 \log \frac{\varepsilon}{C}\right)^\alpha,$$

which yields the following conditions for the exponential asymptotics:

$$(4.21) \quad M = \left\lceil \frac{1}{\alpha} |z|^{1/\alpha} \right\rceil + 1, \quad r_1 = \left(-2 \log \frac{\varepsilon}{C}\right)^\alpha,$$

where $\lceil x \rceil$ is the smallest integer larger than x . The parameter M denotes the number of terms in the series that are taken into account to achieve the given accuracy. \square

Finally it is important to mention that the use of the Berry-type smoothing in the region close to the Stokes lines avoids numerical problems of the asymptotic series in the transition area between \mathbb{G}_2 (with (2.3)) and \mathbb{G}_3 (with (2.4)) and gives a much faster convergence due to the exponential corrections of the series.

4.3. Integral representation.

4.3.1. Basic formulas. For the area between the Taylor series and the exponentially improved asymptotics, Hankel's integral representation can be used for calculating the values of $E_{\alpha,\beta}(z)$. Another approach for calculating the Mittag-Leffler function was suggested in [4], but that algorithm neglects the numerical difficulties that arise for values of z close to the contour path. Also, it does not make use of the exponentially improved asymptotics and hence is much slower. We avoid the problems of [4] near the contour path by using two different integration formulas with different contours. In the following paragraph the integration formula will be derived from Hankel's integral representation by inserting the contour path into the definition, and the behavior of the integrands will be discussed. Finally we present the approximations and the error estimates of the integrals used in the numerical scheme.

We start from the classical Hankel representation of the generalized Mittag-Leffler function which is obtained by inserting the Hankel representation of the inverse Gamma function in the series expansion (2.1). The integral representation is given by [2, p. 210]

$$(4.22) \quad E_{\alpha,\beta}(z) = \frac{1}{2\pi i} \int_C \frac{y^{\alpha-\beta} e^y}{y^\alpha - z} dy,$$

where the path of integration \mathcal{C} in the complex plane starts and ends at $-\infty$ and encircles the circular disc $|y| \leq |z|^{1/\alpha}$ in the positive sense.

Bending the contour in the complex plane and applying the Cauchy theorem, one obtains the following integral representation [21] for $0 < \alpha < 2$:

$$(4.23) \quad E_{\alpha,\beta}(z) = \frac{1}{2\pi i \alpha} \int_{\gamma(\varrho,\vartheta)} \frac{e^{\xi^{1/\alpha}} \xi^{\frac{1-\beta}{\alpha}}}{\xi - z} d\xi \quad \text{for } z \in G^{(-)}(\gamma),$$

$$(4.24) \quad E_{\alpha,\beta}(z) = \frac{1}{\alpha} z^{\frac{1-\beta}{\alpha}} \exp(z^{1/\alpha}) + \frac{1}{2\pi i \alpha} \int_{\gamma(\varrho,\vartheta)} \frac{e^{\xi^{1/\alpha}} \xi^{\frac{1-\beta}{\alpha}}}{\xi - z} d\xi \quad \text{for } z \in G^{(+)}(\gamma),$$

where the contour $\gamma(\varrho, \vartheta)$ starts at infinity in the lower half-plane, goes along a ray of $\arg(z) = -\vartheta$ towards the origin, encircles the origin with a circular arc of radius ϱ , and goes back to infinity in the upper half-plane along the ray $\arg(z) = +\vartheta$. Thus the complex plane is divided by the contour path in two parts, where $G^{(-)}(\gamma)$ and $G^{(+)}(\gamma)$ are the areas left and right of the contour path, respectively. Close to the contour path the numerical evaluation of the formulas (4.23) and (4.24) becomes inaccurate because of the singularity of the integral (4.23) at $r = |z|e^{\pm i\vartheta}$.

Combining formula (4.24) with $\vartheta = \pi\alpha$ and (4.23) with $\vartheta = 2\pi\alpha/3$, one can cover the whole complex plane. The regions $G^{(+)}(\pi\alpha)$ and $G^{(-)}(2\pi\alpha/3)$ have nonvanishing overlap. The overlap allows us to avoid the use of formulas (4.23) and (4.24) close to the contour path by choosing the partitioning described in section 3. The value of ϱ was set to 0.5 and thus lies in \mathbb{G}_1 , where the Taylor series is used for the calculation. Equation (4.24) is used with $\vartheta = \pi\alpha$ for $z \in \mathbb{G}_5$ and (4.23) with $\vartheta = 2\pi\alpha/3$ for $z \in \mathbb{G}_6$. When these integrals are evaluated, several cases arise. We distinguish the cases $\beta \leq 1$ and $\beta > 1$.

Let $z \in \mathbb{G}_5$. Summing up the different terms after inserting the parameterization of the contour path for $\vartheta = \pi\alpha$ and $\varepsilon = 1/2$ yields for $z \in G^{(+)}(\gamma)$ that

$$(4.25) \quad E_{\alpha,\beta}(z) = A(z; \alpha, \beta, 0) + \int_0^\infty B(r; \alpha, \beta, z, \pi\alpha) dr$$

for $\beta \leq 1$ and

$$(4.26) \quad E_{\alpha,\beta}(z) = A(z; \alpha, \beta, 0) + \int_{1/2}^\infty B(r; \alpha, \beta, z, \pi\alpha) dr + \int_{-\pi\alpha}^{\pi\alpha} C(\varphi; \alpha, \beta, z, 1/2) d\varphi$$

for $\beta > 1$, where the following abbreviations are used:

$$(4.27) \quad A(z; \alpha, \beta, x) = \frac{1}{\alpha} z^{(1-\beta)/\alpha} \exp\left[z^{1/\alpha} \cos(x/\alpha)\right],$$

$$(4.28) \quad B(r; \alpha, \beta, z, \phi) = \frac{1}{\pi} A(r; \alpha, \beta, \phi) \frac{r \sin[\omega(r, \phi, \alpha, \beta) - \phi] - z \sin[\omega(r, \phi, \alpha, \beta)]}{r^2 - 2rz \cos \phi + z^2},$$

$$(4.29) \quad C(\varphi; \alpha, \beta, z, \varrho) = \frac{\varrho}{2\pi} A(\varrho; \alpha, \beta, \varphi) \frac{\cos[\omega(\varrho, \varphi, \alpha, \beta)] + i \sin[\omega(\varrho, \varphi, \alpha, \beta)]}{\varrho(\cos \varphi + i \sin \varphi) - z},$$

$$(4.30) \quad \omega(x, y, \alpha, \beta) = x^{1/\alpha} \sin(y/\alpha) + y(1 + (1 - \beta)/\alpha).$$

In the case $\beta \leq 1$ we applied the limit $\varrho \rightarrow 0$. These equations are used to calculate $E_{\alpha,\beta}$ for $z \in \mathbb{G}_5$.

For $z \in \mathbb{G}_6$ we use a different contour with $\vartheta = 2\pi\alpha/3$. In this case the integral representations read

$$(4.31) \quad E_{\alpha,\beta}(z) = \int_0^\infty B(r; \alpha, \beta, z, 2\pi\alpha/3) dr, \quad \beta \leq 1,$$

$$(4.32) \quad E_{\alpha,\beta}(z) = \int_{1/2}^\infty B(r; \alpha, \beta, z, 2\pi\alpha/3) dr + \int_{-2\pi\alpha/3}^{2\pi\alpha/3} C(\varphi; \alpha, \beta, z, 1/2) d\varphi, \quad \beta > 1,$$

where the integrands have been defined in (4.27)–(4.30) above.

The integrand $C(\varphi; \alpha, \beta, z, \varrho)$ is oscillatory but bounded over the integration interval. Thus the integrals over C can be evaluated numerically using any appropriate quadrature formula. We use a robust adaptive 21-point Gauss–Kronrod scheme from the gnu scientific library (GSL) [3], which is based on the QUADPACK QAGS algorithm [14]. Other robust integration schemes such as the standard MATLAB Gauss–Lobatto scheme have also been used successfully. The integrals over $B(r; \alpha, \beta, z, \phi)$ involve unbounded intervals and have to be treated more carefully.

4.3.2. Integrands. As the integral representation is used only for $|z| > 0$, we assume z to be nonzero. It can be easily shown that the integrand $B(r; \alpha, \beta, z, \phi)$ in (4.28) behaves like $\mathcal{O}(r^{\frac{1-\beta}{\alpha}})$ for $r \rightarrow 0$ which yields to the following cases: For $\beta < 1 + \alpha$ the integrand $\int_a^\infty B(r; \alpha, \beta, z, \phi) dr$ is convergent in the limit $a \rightarrow 0$, but the integrand remains finite at $r = 0$ only for $\beta \leq 1$. Thus, for numerical integration the limit $a \rightarrow 0$ can be applied only in the case $\beta \leq 1$ in (4.31). For β exactly $1 + \alpha$ and $\phi = \pi\alpha$, the integrand can be further simplified and approaches a finite value in the limit $r \rightarrow 0$. The integrands for different cases of α and β are shown in Figure 2.

A special case in the integrand in (4.28) occurs when z lies on the contour line. Then the denominator becomes zero which causes problems in the numerical scheme. Although there are numerical algorithms for treating such integrands with singularities, it is much more accurate to avoid such a case if possible. In our case this has been done by choosing two different integral representations with different contour paths, so one can always be used in the case of z close to the contour of the other.

This also speeds up the algorithm because the integrand is smoother and the integration routine does not need to treat the singularities. The behavior of the integrand close to the contour path is shown in Figure 3.

4.3.3. Error estimates. Now we present the error estimates for the different integral formulas. The truncation points for the integrals over $B(r; \alpha, \beta, z, \phi)$ are determined such that the error $R(R_{\max}; \alpha, \beta, z, \phi)$ is smaller than a given accuracy ε .

For given $z \in \mathbb{G}_5$ (resp., $z \in \mathbb{G}_6$) and accuracy ε , we approximate the integrals by truncation. The error

$$(4.33) \quad R(R_{\max}; \alpha, \beta, z, \phi) \leq \left| \int_{R_{\max}}^\infty B(r; \alpha, \beta, z, \phi) dr \right| < \varepsilon$$

depends on the truncation point R_{\max} .

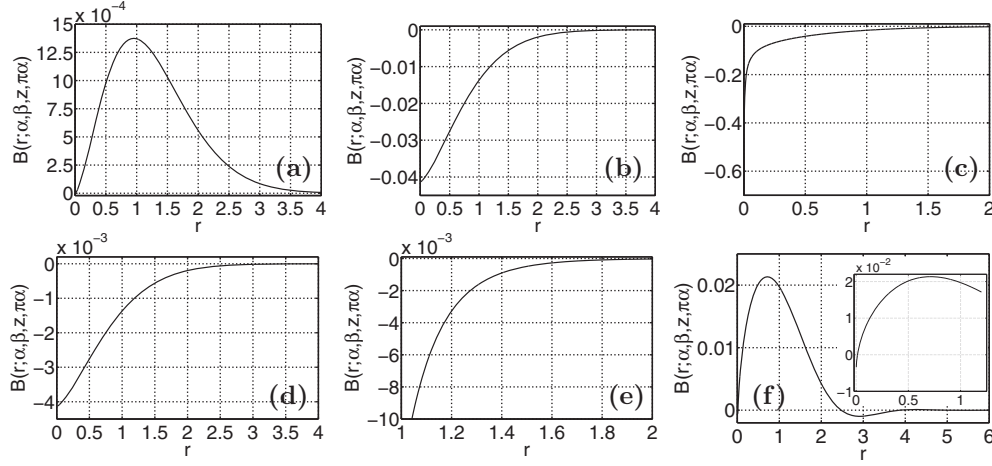


FIG. 2. (a)–(e) summarize the behavior of the integrand $B(r; \alpha, \beta, z, \phi)$ for different combinations of α and β , where $\phi = \pi\alpha$ and $z = 10$ are kept constant. (a) $\beta < 1$, $\beta < 1 + \alpha$: In this case the integral is convergent and the integrand approaches 0 for $r \rightarrow 0$. For the plot $\alpha = \beta = 2/3$ was chosen. (b) $\beta = 1$, $\beta < 1 + \alpha$: For $\beta = 1$ the integrand approaches a finite value in the limit $r \rightarrow 0$. The parameters for the figure are $\alpha = 2/3$ and $\beta = 1$. (c) $\beta > 1$, $\beta < 1 + \alpha$: If $\beta > 1$ but still smaller than $1 + \alpha$, the integral is still convergent but the integrand diverges in the limit $r \rightarrow 0$. The values for the plot have been chosen as $\alpha = 2/3$ and $\beta = 5/4$. (d) $\beta = 1 + \alpha$: This is a special case where the integrand approaches again a finite value in the limit $r \rightarrow 0$. The plot shows the integrand for $\alpha = 2/3$ and $\beta = 5/3$. (e) $\beta > 1 + \alpha$: For $\beta > 1 + \alpha$ the integrand diverges in the limit $r \rightarrow 0$ and the integral over $B(r; \alpha, \beta, z, \phi)$ does not converge anymore. (f) This figure shows the integrand $B(r; \alpha, \beta, z, \phi)$ for another value of $z = -10$ and $\phi = 2\pi\alpha/3$. The parameters α and β were chosen to be $\alpha = 2/3$ and $\beta = 1 + \alpha$. In this case the integrand does not approach a finite value in the limit $r \rightarrow 0$ as in the case $\phi = \pi\alpha$.

Inserting $\phi = \pi\alpha$ (resp., $\phi = 2\pi\alpha/3$) in $B(r; \alpha, \beta, z, \phi)$ one obtains, after simplifying the resulting terms,

$$(4.34) \quad B(r; \alpha, \beta, z, \pi\alpha) = \frac{1}{\pi\alpha} r^{(1-\beta)/\alpha} e^{-r^{1/\alpha}} \times \frac{r \sin[\pi(1-\beta)] - z \sin[\pi(1-\beta+\alpha)]}{r^2 - 2rz \cos \phi + z^2},$$

$$(4.35) \quad B(r; \alpha, \beta, z, 2\pi\alpha/3) = \frac{1}{\pi\alpha} r^{(1-\beta)/\alpha} e^{-(1/2)r^{1/\alpha}} \times \frac{r \sin[\omega(r, \frac{2\pi\alpha}{3}, \alpha, \beta) - \frac{2\pi\alpha}{3}] - z \sin[\omega(r, \frac{2\pi\alpha}{3}, \alpha, \beta)]}{r^2 - 2rz \cos \phi + z^2},$$

where $\omega(r, \frac{2\pi\alpha}{3}, \alpha, \beta) - \frac{2\pi\alpha}{3} = r^{1/\alpha} \frac{\sqrt{3}}{2} + \frac{2\pi}{3}(1-\beta)$ and $\omega(r, \frac{2\pi\alpha}{3}, \alpha, \beta) = r^{1/\alpha} \frac{\sqrt{3}}{2} + \frac{2\pi}{3}(\alpha + (1-\beta))$.

If we assume $r \geq 2|z|$, one finds for the denominator of (4.34) and (4.35) that

$$(4.36) \quad \frac{1}{|r^2 - 2rz \cos \phi + z^2|} = \frac{1}{r^2 \left| \frac{z}{r} - z_0 \right| \left| \frac{z}{r} - \bar{z}_0 \right|} \leq \frac{1}{r^2 \left(\left| \frac{z}{r} \right| - z_0 \right) \left(\left| \frac{z}{r} \right| - \bar{z}_0 \right)} \leq \frac{4}{r^2},$$

where ϕ is either $\pi\alpha$ or $2\pi\alpha/3$ and $z_0 = e^{i\phi}$.

As α, β, r , and ϕ are real numbers, one easily obtains

$$(4.37) \quad \left| \sin[\omega(r, \phi, \alpha, \beta) - \phi] - z \sin[\omega(r, \phi, \alpha, \beta)] \right| \leq \frac{3r}{2}$$

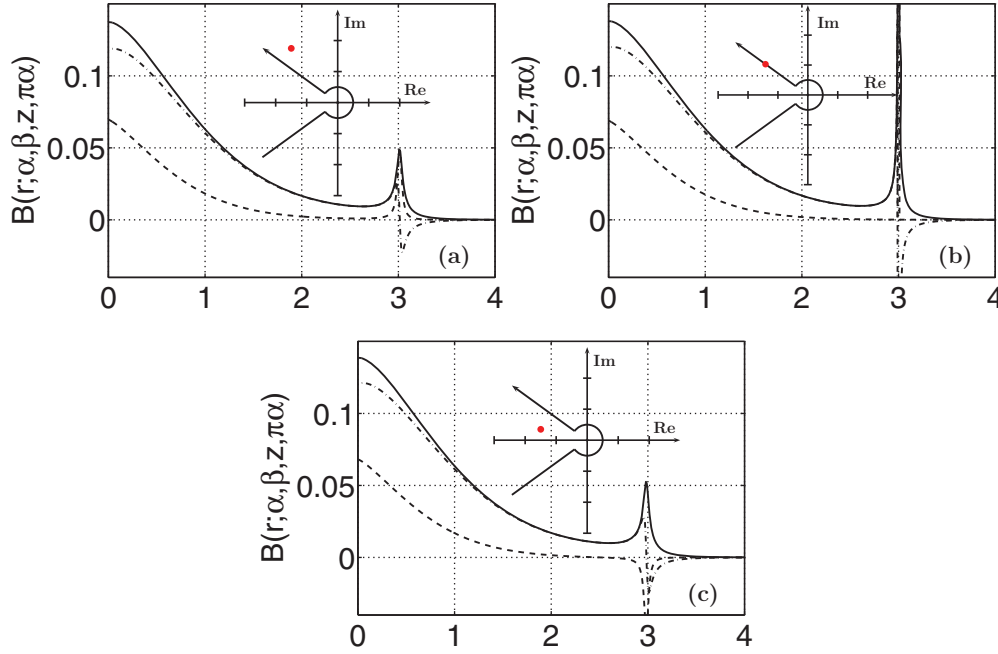


FIG. 3. The three plots show the divergence of the integrand $B(r; \alpha, \beta, z, \phi)$ close to the contour path. The real part is drawn with a dashed line and the imaginary part with a dashed-dotted line. The absolute value is marked with a black solid line. The parameters in the figures are $\alpha = 2/3$, $\beta = 1$, and $\phi = \pi\alpha$. (a) shows the integrand for z slightly above the contour path ($z = \exp(i\pi\alpha) + 0.03$), while in (c) the integrand is shown for slightly below ($z = \exp(i\pi\alpha) - 0.03$). The singularity is shown in (b) when z lies on the contour path. The insets show the contour path for the integration and the location of z relative to the contour path as a black dot.

for the numerator because in (4.36) r was assumed to be larger than $2|z|$. The angle ϕ is either $\pi\alpha$ or $2\pi\alpha/3$. Thus we obtain for the integrals

$$(4.38) \quad \left| \int_{R_{\max}}^{\infty} B(r; \alpha, \beta, z, \pi\alpha) dr \right| \leq \int_{R_{\max}}^{\infty} \frac{6}{\pi\alpha} r^{\frac{(1-\beta)}{\alpha}-1} e^{-r^{1/\alpha}} dr$$

$$\leq \frac{6}{\pi} \Gamma(1 - \beta, R_{\max}^{1/\alpha}),$$

$$(4.39) \quad \left| \int_{R_{\max}}^{\infty} B(r; \alpha, \beta, z, 2\pi\alpha/3) dr \right| \leq \int_{R_{\max}}^{\infty} \frac{6}{\pi\alpha} r^{\frac{(1-\beta)}{\alpha}-1} e^{-\frac{1}{2}r^{1/\alpha}} dr$$

$$\leq \frac{12}{2\beta\pi} \Gamma\left(1 - \beta, \frac{1}{2}R_{\max}^{1/\alpha}\right)$$

after comparing with the definition of the incomplete gamma function. Now we apply the following two lemmas.

THEOREM 4.3 (lemma). *For the incomplete gamma function the following bounds hold:*

$$(4.40) \quad |\Gamma(1 - \beta, x)| \leq e^{-x} \quad \text{if } x \geq 1, \beta \geq 0,$$

$$(4.41) \quad |\Gamma(1 - \beta, x)| \leq (|\beta| + 2)x^{-\beta} e^{-x} \quad \text{if } x \geq |\beta| + 1, \beta < 0.$$

Proof. For $t \geq x \geq 1$ and $\beta \geq 0$ we have the inequality

$$(4.42) \quad t^{-\beta} e^{-t} \leq e^{-t},$$

and therefore

$$(4.43) \quad |\Gamma(1 - \beta, x)| \leq \int_x^\infty e^{-t} dt = e^{-x},$$

which proves the first inequality (4.40). For $\beta < 0$ we can find an $n \in \mathbb{N}$ such that

$$(4.44) \quad -(n + 1) \leq \beta < -n.$$

For $x > 0$ and $\beta < 0$ it holds that

$$(4.45) \quad \Gamma(1 - \beta, x) = x^{-\beta} e^{-x} \int_0^\infty e^{-u} (1 + (u/x))^{-\beta} du < x^{-\beta} e^{-x} \int_0^\infty e^{-u} (1 + (u/x))^N du,$$

where $N = |\beta| + 1$. This can be shown by using the binomial theorem for expanding $(1 + (u/x))^N$ and integrating (4.45) term by term:

$$(4.46) \quad \Gamma(1 - \beta, x) < x^{-\beta} e^{-x} \left(1 + \frac{N}{x} + N^2 x^2 + \dots + N^N x^N \right) < x^{-\beta} e^{-x} (N + 1),$$

where $x \geq N$ and $N + 1 \leq 2 - \beta$. This yields the second inequality of (4.41):

$$(4.47) \quad |\Gamma(1 - \beta, x)| \leq (|\beta| + 2)x^{-\beta} e^{-x}. \quad \square$$

THEOREM 4.4 (lemma). *The inequality*

$$(4.48) \quad x^y \leq (qy)^y e^{x/q}$$

holds for arbitrary $x, y, q > 0$.

Proof. Let $x = a \cdot y$ with $a > 0$. Then one can write (4.48) as $(ay)^y \leq (qy)^y e^{ay/q}$, which is equivalent to $a^y \leq q^y e^{ay/q}$. Dividing this by q^y and applying the logarithm on both sides yields $y \log(a/q) \leq y(a/q)$, which is the same as $\log(a/q) \leq (a/q)$ because $y > 0$. The last inequality is true because $\log(x) < x \forall x > 0$ and $a, q > 0$. \square

Using Theorem 4.3 with (4.38) (resp., (4.39)) and then applying Theorem 4.4 in the case $\beta < 0$, the following estimates for $\phi = \pi\alpha$ and $\phi = 2\pi\alpha/3$ are obtained:

$$(4.49) \quad R(R_{\max}; \alpha, \beta, z, \pi\alpha) \leq \begin{cases} \frac{6}{\pi} e^{-R_{\max}^{1/\alpha}}, & \beta \geq 0, R_{\max} \geq 1, \\ \frac{6}{\pi} (|\beta| + 2)(2|\beta|)^{|\beta|} e^{-\frac{1}{2}R_{\max}^{1/\alpha}}, & \beta < 0, R_{\max}^{1/\alpha} \geq |\beta| + 1, \end{cases}$$

$$(4.50) \quad R(R_{\max}; \alpha, \beta, z, 2\pi\alpha/3) \leq \begin{cases} \frac{12}{2^{\beta}\pi} e^{-\frac{1}{2}R_{\max}^{1/\alpha}}, & \beta \geq 0, R_{\max} \geq 1, \\ \frac{12}{2^{\beta}\pi} (|\beta| + 2)(4|\beta|)^{|\beta|} e^{-\frac{1}{4}R_{\max}^{1/\alpha}}, & \beta < 0, \\ & R_{\max}^{1/\alpha} \geq |\beta| + 1. \end{cases}$$

In the case $\phi = \pi\alpha$ we applied Theorem 4.4 with $x = R_{\max}^{1/\alpha}$, $y = -\beta$, and $q = 2$, whereas in the case $\phi = 2\pi\alpha/3$ Theorem 4.4 was used with the parameters $x = R_{\max}^{1/\alpha}$, $y = -\beta$, and $q = 4$.

Recalling that (4.36) requires $R_{\max} > 2|z|$ and solving (4.49) and (4.50) for the truncation point R_{\max} , one finds for $\phi = \pi\alpha$ that

$$(4.51) \quad R_{\max} \geq \begin{cases} \max \left\{ 1, 2|z|, \left(-\ln \frac{\pi\varepsilon}{6} \right)^\alpha \right\}, & \beta \geq 0, \\ \max \left\{ (|\beta| + 1)^\alpha, 2|z|, \left(-2 \ln \left(\frac{\pi\varepsilon}{6(|\beta| + 2)(2|\beta|)^{|\beta|}} \right) \right)^\alpha \right\} & \beta < 0 \end{cases}$$

while for $\phi = 2\pi\alpha/3$ we have

$$(4.52) \quad R_{\max} \geq \begin{cases} \max \left\{ 2^\alpha, 2|z|, \left(-2 \ln \frac{\pi 2^\beta \varepsilon}{12} \right)^\alpha \right\}, & \beta \geq 0, \\ \max \left\{ [2(|\beta| + 1)]^\alpha, 2|z|, \left[-4 \ln \frac{\pi 2^\beta \varepsilon}{12(|\beta| + 2)(4|\beta|)^{|\beta|}} \right]^\alpha \right\}, & \beta < 0. \end{cases}$$

5. Discussion of the algorithm. In this section we briefly summarize the algorithm and the different cases that have to be distinguished to calculate $E_{\alpha,\beta}$ for a given error ε . Also the numerical treatment of the constants and error terms is described and details of the algorithm are discussed.

For $|z| \leq 0.95$ the Taylor series (2.1) is used for all $\alpha > 0$ and $\beta \in \mathbb{R}$. We apply the recursion formula (2.2) in the case $\alpha > 1$. The maximum number of terms M in the Taylor series which are needed to achieve an accuracy of ε is given by (4.5). This number increases rapidly for $z \rightarrow 1$; thus the Taylor series becomes inefficient for the calculation of $E_{\alpha,\beta}$ if $z > 0.95$. Furthermore if M becomes very large, the calculation of the gamma function fails due to numerical overflows. This can be avoided by using the identity

$$(5.1) \quad z^k / \Gamma(\alpha k + \beta) = \exp(k \ln(z) - \ln \Gamma(\alpha k + \beta)),$$

which behaves in a more stable manner for large k and $|z|$ not too close to the origin, where the logarithm is singular. Thus for very small $|z| < 0.5$ we switch back to the definition (2.1). In this case only a few terms of the Taylor series are necessary to obtain good accuracy, so one does not have to worry about M . Also a real Lanczos approximation [3] of the reciprocal gamma function is used to avoid problems at the poles of $\Gamma(\alpha k + \beta)$ when β is smaller than 0.

The integral formulas are limited only by the floating arithmetic of the computer, where errors can accumulate due to the rounding errors of the numerical integration scheme.

Now if $|z| \geq r_1$, where r_1 is given by (4.21), the asymptotic formulas are used, where we distinguish between the two asymptotic formulas (2.3) in \mathbb{G}_1 (resp., (2.4) in \mathbb{G}_2) and the Berry-type smoothed regions \mathbb{G}_3 and \mathbb{G}_4 in an angle of $\pm\delta$ around the Stokes lines ((2.5) and (2.6)). In the algorithm we choose $\delta = \pi\alpha/8$ to avoid coming too close to the Stokes lines with (2.3) (resp., (2.4)). For $|\delta| \leq \pi\alpha/8$ the argument $\theta \in [-\pi/8, \pi/8]$ is sufficiently small that one can apply the approximation $c \approx \theta + \frac{1}{6}\theta^2 - \frac{1}{36}\theta^3$. Figure 4 shows a plot of $c(\theta)$. The error of the approximation is much smaller than 1×10^{-4} in the real part and 1×10^{-3} in the imaginary one so that this approximation in the exponent is negligible.

For large α ($\alpha \geq 8/9$) the angle $\pi\alpha + \delta$ would cross the negative real axis and produce a jump in θ ; thus we always make use of the normal asymptotic series in a

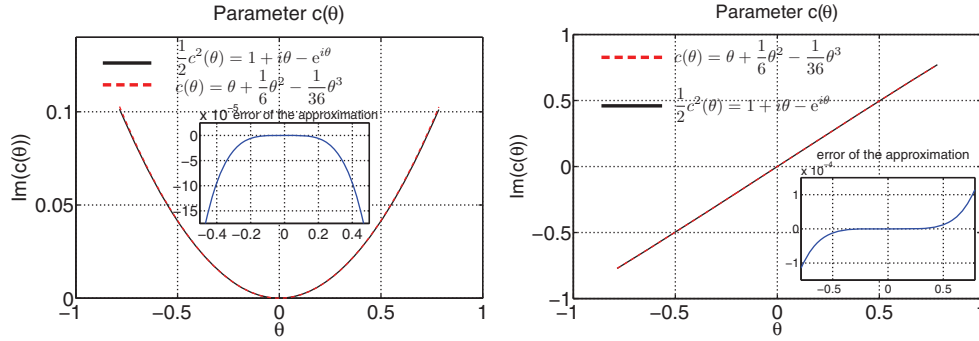


FIG. 4. The figures show the real (left) and imaginary part (right) of the parameter $c(\theta)$ of the Berry-type smoothed asymptotic series (2.5) (resp., (2.6)). The exact solution of $c(\theta)^2/2 = 1 + i\theta - e^{i\theta}$ is plotted as a black solid line, and the approximation $c \approx \theta + \frac{1}{6}\theta^2 - \frac{1}{36}\theta^3$ is marked with a dashed line. In the considered region of $\theta \in [-\pi/4, \pi/4]$ the difference between the two curves is negligible. The absolute error of the approximation is given in the inset plot.

wedge around the negative real axis, where the opening angle $\tilde{\delta}$ is between $\pi\alpha$ and π . More precisely $\tilde{\delta}$ is defined by $\tilde{\delta} = \min\{(\pi + \pi\alpha)/2, \delta\}$, where δ is the angle of the wedge around the Stokes line (cf. (3.7)). In the algorithm δ was chosen to be $\pi\alpha/8$.

Optimal truncation for the series should be achieved for M according to (4.21), which would mean that the number of necessary coefficients will increase with $\sim |z|^{1/\alpha}$. But for $z \rightarrow \infty$ the asymptotic series becomes better and better, so we apply an upper limit of $M < 100$ in the algorithm. This is also necessary to avoid overflows in the reciprocal gamma function for small negative values which reaches the floating point limit for about $\beta - \alpha k \approx 130$. As the term $z^{-k}/\Gamma(\beta - \alpha k)$ involves the multiplication of a very small number ($z^{-k} \ll 1$) with a very large number $1/\Gamma(\beta - \alpha k) \gg 1$, it is better to apply the $\exp - \log$ identity again for large k . In this case the calculation of $\log \Gamma(\beta - \alpha k)$ can fail due to the poles of the gamma function for negative integer values; thus we assume all terms to be zero for which $\beta - \alpha k$ is closer than 10^{-9} to a negative integer value.

In the algorithm the constant C in (4.19) is replaced with

$$(5.2) \quad C_0 = \frac{1}{2\pi} \left(\frac{1}{\sin \alpha\pi} + \frac{1}{\min\{\sin \alpha\pi, \sin \xi\}} \right) \approx \frac{1}{\pi \sin \pi\alpha},$$

obtained by combining (4.11) and (4.12). The choice to limit the constant C_0 on the Stokes line is supported analytically by the argument of Boyd [1, 23] that demands a smooth transition when crossing the Stokes line from one side to the other. Therefore the error cannot diverge when ξ goes to zero. Extensive numerical tests (see Table 2) and comparisons with the integral representations show that with (5.2) the relative errors between the asymptotic series and the integral representation are extremely small for $|z| \leq r_1 = (-2 \log(\varepsilon/C_0))^\alpha$. In practice the influence of the exact numerical value of C_0 is small as the constant appears inside a logarithm. In the Berry-type smoothed regions, the series (2.5) and (2.6) shows even better, namely, exponential convergence, than the normal series. Thus we can use the same estimate for r_1 as under optimal truncation.

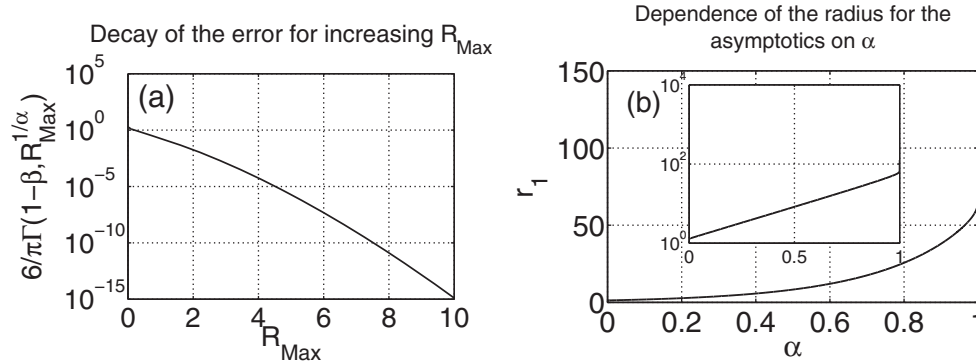


FIG. 5. The two plots summarize the results of the error estimates of the integral representation. (a) shows the decay of the error term (4.38) of the integral representation for $\alpha = \beta = 2/3$ on a semilog scale. It decays faster than exponentially with R_{max} . (b) shows the dependence of the radius r_1 on the parameter α for a given tolerance $\varepsilon = 1e - 12$ using the formula $r_1 = (-2\log(\varepsilon/C_0))^\alpha = 14.16$, with C_0 given by (5.2). The radius r_1 determines from where on the asymptotic formula that is used to calculate $E_{\alpha,\beta}(z)$. The inset shows a semilogarithmic plot of the same region.

If $0.95 < |z| < r_1$, the integral formulas are used in \mathbb{G}_5 and \mathbb{G}_6 . For the error estimates we have to distinguish here $\beta > 1$ and $\beta \leq 1$, where the case $\beta \leq 1$ yields two further subcases $\beta \geq 0$ and $\beta < 0$. The contours for the integral formulas for the areas \mathbb{G}_5 and \mathbb{G}_6 have been chosen such that z will never come close to the contour of integration. A plot of the areas \mathbb{G}_5 and \mathbb{G}_6 with the two contour paths $\gamma(1/2, \pi\alpha)$ and $\gamma(1/2, 2\pi\alpha/3)$ is shown in Figure 1(b). Figure 5(a) shows a plot of the right-hand side of (4.38) versus R_{max} . One can see that the accuracy is extremely good even for rather small R_{max} . The estimates for R_{max} are given in (4.51) and (4.52).

The integrand in (4.29) is oscillatory. The amplitude of these oscillations is mainly determined by the prefactor in (4.27). For real argument $z \in \mathbb{R}$, the imaginary part of the integrand is antisymmetric in (4.27) with respect to the origin. This means that the integral over the imaginary part of (4.29) vanishes and does not have to be calculated. For the real part one can also make use of the symmetry and perform the integration over only half of the contour arc.

A detailed description of the behavior of the generalized Mittag-Leffler function in the complex plane and the investigation of the distribution of the zeros can be found in [7]. Two contour plots of $E_{\alpha,\beta}(z)$ are shown in Figure 6.

The algorithm has been implemented for complex z with real and imaginary parts in double precision. The parameters α and β are represented as real double variables. A separate function for real double z has also been implemented. In this case the integration routines make use of the symmetry of the integrand and the fact that $\text{Im}(E_{\alpha,\beta}(x)) = 0$. This speeds up the integration routine and improves the stability of the algorithm.

6. Numerical tests and speed analysis of the algorithm. Extensive numerical calculations of the algorithm were performed to test the stability and the validity range for the parameters $\alpha, \beta \in \mathbb{R}$ and the argument $z \in \mathbb{C}$. The results are summarized in this section.

By incorporating the asymptotic formula the algorithm has been much improved. Especially for large values of $|z|$ the asymptotic series are much faster and more stable than the integral formulas. For some representative values the differences are reported

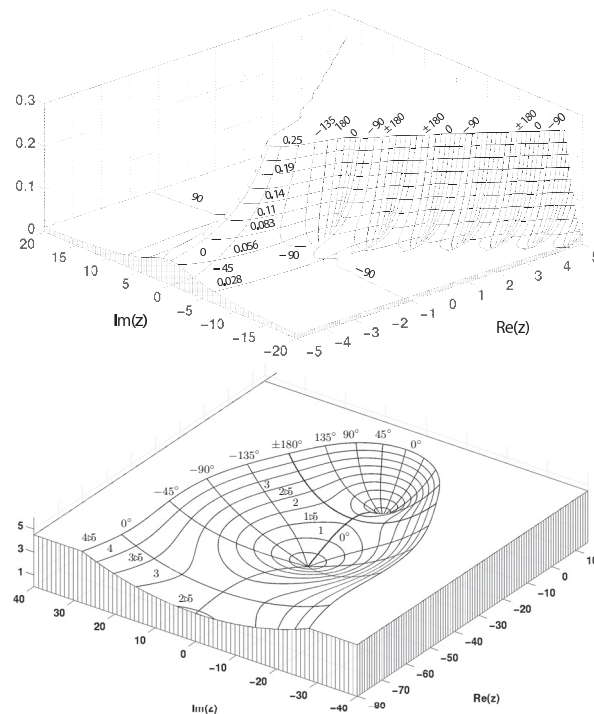


FIG. 6. The plots show the behavior of the Mittag-Leffler function $E_{\alpha,1}(z)$ in the complex plane for $\alpha = 0.8$ (top) and $\alpha = 2.25$ (bottom). In the three-dimensional plot the absolute value of the function is plotted with the contour lines on top. Furthermore, the contour lines of the argument are also marked.

in Table 1, where the speed of the integral routine is compared to the asymptotic formula in a range where both formulas can be used for the calculation. The speedup factor ranges typically between 20 and 40. Close to the Stokes lines the Berry-type smoothed formulas give a better approximation than the normal asymptotic series.

The convergence of the series is compared with the values obtained by the integral representation along rays with constant argument for $|z| \rightarrow \infty$. Good agreement and fast convergence is obtained in all sectors of the complex plane.

For very large values of $|z|$ the integral formula cannot be used due to rounding errors in the floating point arithmetic. Also the dependence on the parameters α and β is very important; for example, the amplitude equation (4.27) of the integrand $B(r; \alpha, \beta, z, \delta)$ in (4.28) behaves like $r^{(1-\beta)/\alpha}$. If this value becomes too large, the integration routines cannot achieve the required precision. An example of $B(r; \alpha, \beta, z, \delta)$ for different $\beta = 5, 10, 20$ is shown in Figure 7. Similar limitations hold for the integrand in (4.29), where the integrand oscillates with a higher and higher frequency while the value of the integral is close to zero (see Figure 8).

A comparison of the integral formula with the asymptotic series in a range around r_1 is shown in Figure 9. The range for which we still obtained reasonable results is summarized in Table 2. The tests were performed by calculating the values of $E_{\alpha,\beta}(z)$ on a rectangular grid with $\text{Re}_{\min} \leq \text{Re}(z) < \text{Re}_{\max}$ and $\text{Im}_{\min} \leq \text{Im}(z) < \text{Im}_{\max}$ with different lattice spacings. Furthermore the values of $E_{\alpha,\beta}$ are calculated along different rays from the origin covering the different areas of the partitioning (section 3) of the complex plane. For various combinations of α and β the range of validity with respect

TABLE 1

Comparison of the speedup for the calculation for $E_{\alpha,\beta}$ using the asymptotic series expansions. The tolerance ε is set to 10^{-16} . The last column indicates the equation used for the calculation of the asymptotic series. Each speedup factor is averaged over 100 calculations. All calculations were done using the complex algorithm.

α	β	z	$E_{\alpha,\beta}^{\text{int}}(z)$	$E_{\alpha,\beta}^{\text{int}}(z) - E_{\alpha,\beta}^{\text{asym}}(z)$	Speedup
0.6	0.8	7.0	4.24680224e + 11	0.0	40.8
0.6	0.8	20.0	4.50513132e + 64	0.0	21.1
0.6	0.8	-7.0	0.036402965145	6.2000e - 13	55.5
0.6	0.8	-50.0	0.004463867842	0.0	35.3
0.6	0.8	$7e^{0.6\pi i}$	0.00509750 + 0.03299810i	$1.06e - 12 - 2.28e - 12i$	57.1
0.6	0.8	$20e^{0.6\pi i}$	0.00282134 + 0.01075547i	0.0	39.7
0.6	1.25	7.0	9.86821285e + 10	0	22.0
0.6	1.25	20.0	4.76359640e + 63	0	14.0
0.6	1.25	-7.0	0.101261033685	$4.3e - 13$	31.2
0.6	1.25	-50.0	0.014419766303	0.0	16.01
0.6	1.25	$7e^{0.6\pi i}$	0.03339025 + 0.0980431i	$-8.0e - 14 - 2.70e - 13i$	32.7
0.6	1.25	$20e^{0.6\pi i}$	0.01128945 + 0.0342852i	0.0	16.1
0.6	-0.8	7.0	4.24680224e + 11	0.0	40.8
0.6	-0.8	20.0	4.50513132e + 64	0.0	21.1
0.6	-0.8	-7.0	0.036402965145	$6.2e - 13$	55.5
0.6	-0.8	-50.0	0.004463867842	0.0	35.3
0.6	-0.8	$7e^{0.6\pi i}$	0.01931826 + 0.0537209i	$-4.61e - 10 - 8.36e - 10i$	69.0
0.6	-0.8	$20e^{0.6\pi i}$	0.00592228 + 0.0179734i	0.0	35.2

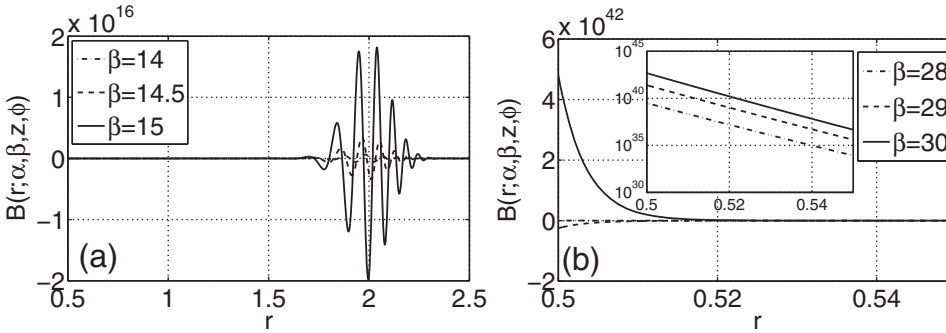


FIG. 7. The figure shows the integrand $B(r; \alpha, \beta, z, 2\pi\alpha/3)$ for $\alpha = 0.2$ and different values of large $|\beta|$. The argument is set to $z = -5 \in \mathbb{G}_5$ (left). One can see how strongly the amplitude increases with increasing β . The oscillations are especially difficult to handle as the large positive parts of the integral cancel out with the large negative ones. The right figure shows the integrand $B(r; \alpha, \beta, z, 2\pi\alpha)$ in the case $z = 5 \in \mathbb{G}_6$ for the parameters $\beta = 28$ to $\beta = 30$. Note the values on the y-axis. In the inset the semilog plot of the absolute value of the integrand in the same range is shown.

to the argument z was determined for the integral representation and the asymptotic series. The upper limit $|z|_{\max}^{\text{int}}$ for which the integral representation is still valid is calculated as follows: Let $E_{\alpha,\beta}^{\text{int}}$ be the values of the Mittag-Leffler function calculated with the integral representation and $E_{\alpha,\beta}^{\text{asym}}$ those obtained from the asymptotic series. As for $|z| \rightarrow \infty$ the asymptotic series becomes more and more accurate; thus the difference $|E_{\alpha,\beta}^{\text{int}} - E_{\alpha,\beta}^{\text{asym}}|$ decreases until it increases again for $|z| > |z|_{\max}^{\text{int}}$ due to the fact that the integral representation becomes inaccurate. For given α and β the value reported in Table 2 is the minimum of all $|z|_{\max}^{\text{int}}$ obtained on the different rays covering all sectors of the partitioning described in section 3.

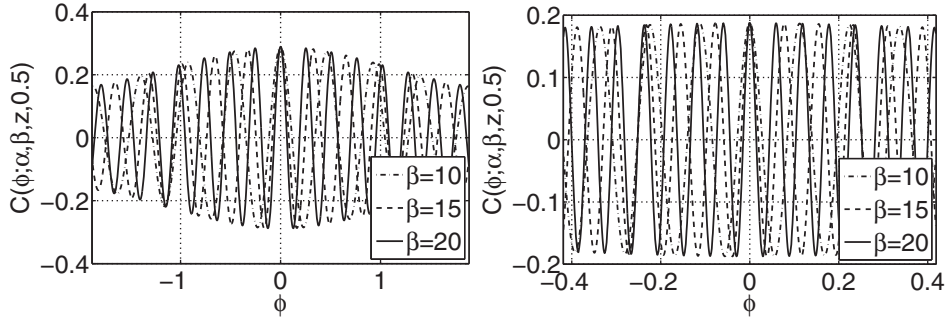


FIG. 8. The figure shows the integrand $C(\varphi; \alpha, \beta, z, \varrho)$ in (4.29) for $\alpha = 0.9$ and different values of β (left). The same integrand but for $\alpha = 0.2$ is shown in the right figure. All other parameters are the same in both plots, where z was set to -5 and $\varrho = 0.5$.

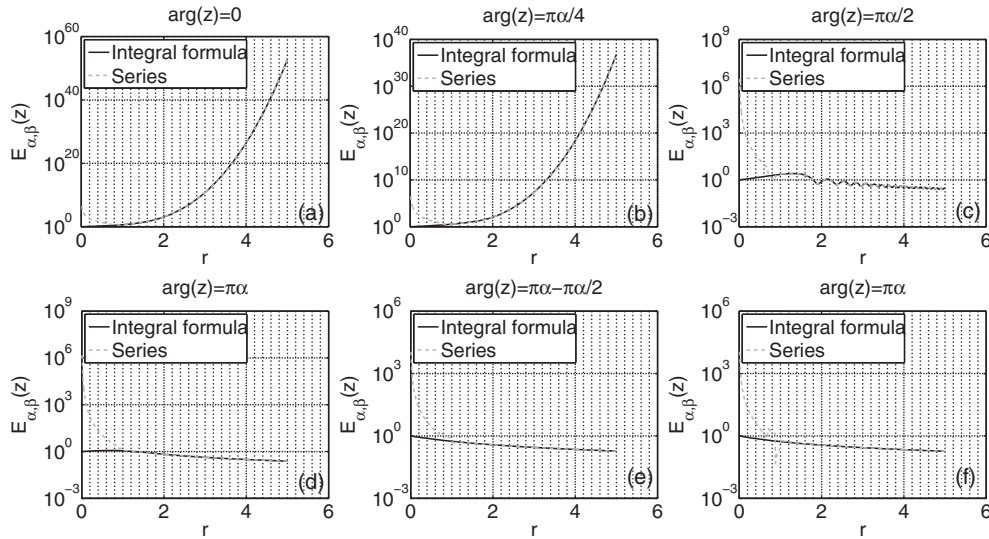


FIG. 9. The figures show the behavior of the Mittag-Leffler function in a range of $|z|$ around r_1 calculated with the asymptotic series (gray dashed line) and the integral formula (black solid line) for different arguments of z . Starting from (a) to (f) the arguments are (a) $\arg(z) = 0$, (b) $\arg(z) = \pi/4$, (c) $\arg(z) = \pi/2$, (d) $\arg(z) = \pi$, (e) $\arg(z) = \pi - \pi/4$, and (f) $\arg(z) = \pi$. The example is calculated for $\alpha = 1/3$, $\beta = 2$, and $\varepsilon = 10^{-10}$. The value of r_1 in this case is $r_1 = (-2 \log(\varepsilon/C))^\alpha = 3.53$.

In the case $|z| \rightarrow 0$ the asymptotic series becomes unstable. The lower bound $|z|_{\min}^{\text{asym}}$ of the asymptotic series is defined by the value of $|z|$ for which the relative error $\text{Err}_{\text{rel}} = |(E_{\alpha,\beta}^{\text{int}} - E_{\alpha,\beta}^{\text{asym}})/E_{\alpha,\beta}^{\text{int}}|$ exceeds 10^{-2} . The largest value of $|z|_{\min}^{\text{asym}}$ along the different rays is shown in Table 2.

For the parameters α and β we find that, in the range $0.05 < \alpha < 0.999$ and $-2 < \beta < 2$, the algorithm covers the whole complex plane up to machine precision in the asymptotic formula which is reached for positive values at $\text{Re}(z) \leq 1.5$ ($\alpha = 0.05$) and $|z| \leq 600$ ($\alpha = 0.999$) as the function grows like $1/\alpha \exp(x^{1/\alpha})$. For $\text{Re}(z) \rightarrow -\infty$ the limits are much larger. For a negative argument the function can be calculated at least for $\text{Re}(z) > -10^{50}$.

TABLE 2

Comparison of the asymptotic series and the integral formula for different combinations of α and β . The value $|z|_{\max}^{\text{int}}$ indicates when the integral formulas start to become inaccurate (see text). For $z < |z|_{\min}^{\text{asym}}$ the asymptotic formula begins to break down. This value is defined by the smallest number of $|z|$ for which the relative error is still smaller than 10^{-2} . The relative error is defined by $\text{Err}_{\text{rel}} = |(E_{\alpha,\beta}^{\text{int}} - E_{\alpha,\beta}^{\text{asym}})/E_{\alpha,\beta}^{\text{int}}|$, where $E_{\alpha,\beta}^{\text{int}}$ are the values of $E_{\alpha,\beta}$ obtained with the integral representation and $E_{\alpha,\beta}^{\text{asym}}$ are the values calculated with the series expansion. The numerical values of the relative error at the points $|z| = r_1$ are reported in the sixth column, where $r_1 = (-2 \log(\varepsilon/C_0))^\alpha$ is the lower radius for the asymptotic series. The value of ε is set to 10^{-11} , and C_0 is given by (5.2).

α	β	$ z _{\max}^{\text{int}}$	$ z _{\min}^{\text{asym}}$	r_1	Err_{rel} at r_1
0.1	-5	$ z _{\max} = 8.5 \pm 0.5$	1.3566	1.4809	1.0835e - 05
0.1	-1	$ z _{\max} = 8.5 \pm 0.5$	1.2718	1.4809	8.7296e - 08
0.1	-2/3	$ z _{\max} = 8.5 \pm 0.5$	1.2380	1.4809	3.2593e - 08
0.1	2/3	> 200	1.1391	1.4809	3.8697e - 10
0.1	1	> 200	1.1052	1.4809	8.2624e - 11
0.1	5/3	$ z _{\max} = 5.5 \pm 0.5$	1.1173	1.4809	3.0580e - 11
0.2	-5	$ z _{\max} = 13.5 \pm 0.5$	1.7785	2.1817	1.8535e - 09
0.2	-1	$ z _{\max} = 12.5 \pm 0.5$	1.6014	2.1817	6.0096e - 12
0.2	-2/3	$ z _{\max} = 12.5 \pm 0.5$	1.5863	2.1817	3.8440e - 12
0.2	2/3	> 200	1.3517	2.1817	7.3541e - 12
0.2	1	> 200	1.2778	2.1817	1.0214e - 12
0.2	5/3	$ z _{\max} = 136.5 \pm 0.5$	1.2304	2.1817	2.3144e - 12
0.5	-5	$ z _{\max} = 53.5 \pm 0.5$	4.4068	6.9547	4.4764e - 13
0.5	-1	$ z _{\max} = 40.5 \pm 0.5$	3.3007	6.9547	7.1942e - 14
0.5	-2/3	$ z _{\max} = 40.5 \pm 0.5$	3.2379	6.9547	5.5955e - 14
0.5	2/3	> 200	2.5417	6.9547	1.4747e - 11
0.5	1	> 200	2.0966	6.9547	1.7497e - 12
0.5	5/3	> 200	1.5969	6.9547	1.5321e - 14
0.5	10	> 200	2.7404	6.9547	7.4421e - 07
0.9	-5	> 200	15.2764	34.2477	3.5560e - 13
0.9	-1	> 200	9.7702	34.2477	1.3282e - 10
0.9	-2/3	$ z _{\max} = 190.5 \pm 0.5$	8.5021	34.2477	4.6096e - 13
0.9	2/3	> 200	6.5593	34.2477	1.0505e - 11
0.9	1	> 200	6.3687	34.2477	6.1782e - 12
0.9	5/3	> 200	3.6252	34.2477	8.7930e - 14
0.9	10	> 200	5.9216	34.2477	6.6471e - 08

The limitations of large $|\beta|$ can be overcome using the following relation:

$$(6.1) \quad z^n E_{\alpha,\beta+n\alpha}(z) = \sum_{k=n}^{\infty} \frac{z^{n+k}}{\Gamma(\alpha(n+k) + \beta)} = E_{\alpha,\beta}(z) - \sum_{k=0}^n \frac{z^k}{\Gamma(\alpha k + \beta)}.$$

This extends the range of β to arbitrary large and small values.

7. Conclusion. A numerical algorithm for calculating the generalized Mittag-Leffler function for arbitrary real parameters $\alpha > 0$ and β was presented, and the error estimates have been calculated. Different representations have been used for different values of $z \in \mathbb{C}$ to obtain optimal stability and accuracy. The algorithm is not only fast, but it also eliminates numerical instabilities in other codes [4]. Furthermore the algorithm was extended using exponentially improved asymptotics. The Berry-type smoothing was used to avoid numerical instabilities close to the Stokes lines, where the asymptotic formulas fail. A great improvement in the speed and stability of the algorithm especially for large values of z has been achieved using the asymptotic series as presented in section 6. Furthermore the algorithm has been analyzed in detail, and

several numerical techniques have been discussed to improve the calculation. Finally, a detailed analysis of the numerical stability and validity of the algorithm is given. The algorithm is available as in C and as a MATLAB script for download [20].

Acknowledgments. The authors thank Julian Engel for useful discussions and performing extensive test runs with the algorithm. Furthermore, we want to thank the referees for their constructive criticism and useful hints.

REFERENCES

- [1] W. C. BOYD, *Stieltjes transforms and the Stokes phenomenon*, Proc. R. Soc. Lond. Ser. A Math. Phys. Eng. Sci., 429 (1990), pp. 227–246.
- [2] A. ERDELYI, *Higher Transcendental Functions*, Vols. I–III, Krieger, Malabar, FL, 1981.
- [3] M. GALASSI, *The GNU Scientific Library*, Network Theory Ltd., Bristol, UK, 2006.
- [4] R. GORENFLO, Y. LUCHKO, AND I. LOUTCHKO, *Computation of the Mittag-Leffler function $E_{\alpha,\beta}(z)$ and its derivatives*, Fract. Calc. Appl. Anal., 5 (2002), pp. 491–518. Erratum: Fract. Calc. Appl. Anal., 6 (2003).
- [5] R. HILFER AND L. ANTON, *Fractional master equation and fractal time random walks*, Phys. Rev. E, 51 (1995), pp. 848–851.
- [6] R. HILFER, R. METZLER, A. BLUMEN, AND J. KLAFTER, *Strange kinetics*, Chem. Phys., Special Issue, 284 (2002), pp. 1–2.
- [7] R. HILFER AND H. SEYBOLD, *Computation of the generalized Mittag-Leffler function and its inverse in the complex plane*, Integral Transforms Spec. Funct., 17 (2006), pp. 637–652.
- [8] R. HILFER, *Applications of Fractional Calculus in Physics*, World Scientific, Singapore, 2000.
- [9] R. HILFER, *Experimental evidence for fractional time evolution in glass forming materials*, Chem. Phys., 284 (2002), pp. 399–408.
- [10] G. MITTAG-LEFFLER, *Sur la nouvelle fonction $E_\alpha(x)$* , C. R. Math. Acad. Sci. Paris, 137 (1903), p. 554.
- [11] G. MITTAG-LEFFLER, *Une généralisation de l'intégrale de Laplace-Abel*, C. R. Math. Acad. Sci. Paris, 136 (1903), p. 537.
- [12] G. MITTAG-LEFFLER, *Sur la représentation d'une branche uniforme d'une fonction monogène*, Acta Math., 29 (1905), p. 101.
- [13] R. PARIS, *Exponential asymptotics of the Mittag-Leffler function*, Proc. R. Soc. Lond. Ser. A Math. Phys. Eng. Sci., 458 (2002), pp. 3041–3052.
- [14] E. PIESSENS, E. DE DONCKER-KAPENGER, C. UEBERHUBER, AND D. KAHANER, *Quadpack, a subroutine package for automatic integration*, Springer, New York, 1983.
- [15] I. POLDUBNY, *Fractional Differential Equations*, 1st ed., Academic Press, New York, 1999.
- [16] H. POLLARD, *The completely monotonic character of the Mittag-Leffler function*, Bull. Amer. Math. Soc., 54 (1948), pp. 1115–1116.
- [17] S. SAMKO, K. KILBAS, AND O. MARICHEV, *Fractional Integrals and Derivatives*, Gordon and Breach, Berlin, 1993.
- [18] W. SCHNEIDER, *Completely monotone generalized Mittag-Leffler functions*, Expo. Math., 14 (1996), p. 3.
- [19] H. SEYBOLD AND R. HILFER, *Numerical results for the generalized Mittag-Leffler function*, Fract. Calc. Appl. Anal., 8 (2005), pp. 127–139.
- [20] H. SEYBOLD AND R. HILFER, <http://www.icp.uni-stuttgart.de/~hilfer/forschung>.
- [21] A. WIMAN, *Über den Fundamentalsatz in der Theorie der Funktionen $E_\alpha(x)$* , Acta Math., 29 (1905), pp. 191–201.
- [22] A. WIMAN, *Über die Nullstellen der Funktionen $E_\alpha(x)$* , Acta Math., 29 (1905), pp. 217–234.
- [23] R. WONG AND Y. ZHAO, *Exponential asymptotics of the Mittag-Leffler function*, Constr. Approx., 18 (2002), pp. 355–385.
- [24] W. WYSS, *The fractional diffusion equation*, J. Math. Phys., 27 (1986), pp. 2782–2785.